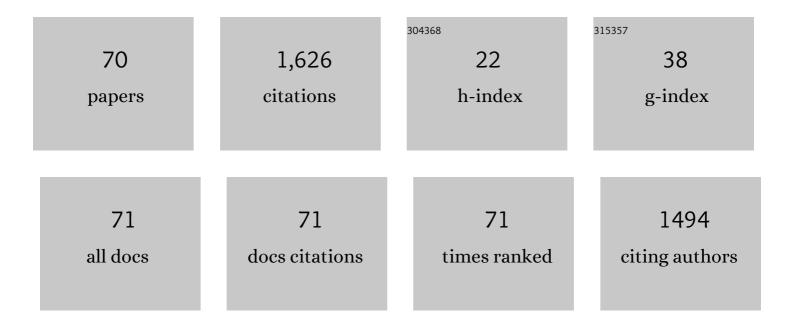
## Taekyung Lee

List of Publications by Year in descending order

Source: https://exaly.com/author-pdf/3156361/publications.pdf Version: 2024-02-01



#	Article	IF	CITATIONS
1	Work hardening associated with É≻martensitic transformation, deformation twinning and dynamic strain aging in Fe–17Mn–0.6C and Fe–17Mn–0.8C TWIP steels. Materials Science & Engineering A: Structural Materials: Properties, Microstructure and Processing, 2011, 528, 7310-7316.	2.6	185
2	Anisotropic properties of directed energy deposition (DED)-processed Ti–6Al–4V. Journal of Manufacturing Processes, 2016, 24, 397-405.	2.8	104
3	Surface Modification of Multipass Caliber-Rolled Ti Alloy with Dexamethasone-Loaded Graphene for Dental Applications. ACS Applied Materials & Interfaces, 2015, 7, 9598-9607.	4.0	82
4	Effects of vanadium carbides on hydrogen embrittlement of tempered martensitic steel. Metals and Materials International, 2016, 22, 364-372.	1.8	71
5	Tensile deformation behavior of Fe–Mn–C TWIP steel with ultrafine elongated grain structure. Materials Letters, 2012, 75, 169-171.	1.3	69
6	Space-holder effect on designing pore structure and determining mechanical properties in porous titanium. Materials & Design, 2014, 57, 712-718.	5.1	64
7	Grain refinement effect on cryogenic tensile ductility in a Fe–Mn–C twinning-induced plasticity steel. Materials & Design, 2013, 49, 234-241.	5.1	61
8	Enhancing tensile properties of ultrafine-grained medium-carbon steel utilizing fine carbides. Materials Science & Engineering A: Structural Materials: Properties, Microstructure and Processing, 2011, 528, 6558-6564.	2.6	59
9	Constitutive analysis of electrically-assisted tensile deformation of CP-Ti based on non-uniform thermal expansion, plastic softening and dynamic strain aging. International Journal of Plasticity, 2017, 94, 44-56.	4.1	50
10	Microstructure tailoring to enhance strength and ductility in Ti–13Nb–13Zr for biomedical applications. Scripta Materialia, 2013, 69, 785-788.	2.6	45
11	Role of Cu on hydrogen embrittlement behavior inÂFe–Mn–C–Cu TWIP steel. International Journal of Hydrogen Energy, 2015, 40, 7409-7419.	3.8	45
12	Tailoring strength-ductility balance of caliber-rolled AZ31 Mg alloy through subsequent annealing. Journal of Magnesium and Alloys, 2020, 8, 163-171.	5.5	41
13	Increased resistance to hydrogen embrittlement in high-strength steels composed of granular bainite. Materials Science & Engineering A: Structural Materials: Properties, Microstructure and Processing, 2017, 700, 473-480.	2.6	38
14	Improved tensile properties of AZ31 Mg alloy subjected to various caliber-rolling strains. Journal of Magnesium and Alloys, 2019, 7, 381-387.	5.5	38
15	Breaking the limit of Young's modulus in low-cost Ti–Nb–Zr alloy for biomedical implant applications. Journal of Alloys and Compounds, 2020, 828, 154401.	2.8	38
16	Role of Mo/V carbides in hydrogen embrittlement of tempered martensitic steel. Corrosion Reviews, 2015, 33, 433-441.	1.0	34
17	Microstructural evolution and strain-hardening behavior of multi-pass caliber-rolled Ti–13Nb–13Zr. Materials Science & Engineering A: Structural Materials: Properties, Microstructure and Processing, 2015, 648, 359-366.	2.6	31
18	Manufacturing Ultrafine-Grained Ti-6Al-4V Bulk Rod Using Multi-Pass Caliber-Rolling. Metals, 2015, 5, 777-789.	1.0	24

TAEKYUNG LEE

#	Article	IF	CITATIONS
19	Effect of Al addition on low-cycle fatigue properties of hydrogen-charged high-Mn TWIP steels. Materials Science & Engineering A: Structural Materials: Properties, Microstructure and Processing, 2016, 677, 421-430.	2.6	24
20	Effect of the amount and temperature of prestrain on tensile and low-cycle fatigue properties of Fe-17Mn-0.5C TRIP/TWIP steel. Materials Science & Engineering A: Structural Materials: Properties, Microstructure and Processing, 2017, 696, 493-502.	2.6	24
21	Comparative study on the effects of Cr, V, and Mo carbides for hydrogen-embrittlement resistance of tempered martensitic steel. Scientific Reports, 2019, 9, 5219.	1.6	24
22	Enhanced yield symmetry and strength-ductility balance of caliber-rolled Mg–6Zn-0.5Zr with ultrafine-grained structure andÂbulk dimension. Journal of Alloys and Compounds, 2019, 803, 434-441.	2.8	22
23	High-Strength AZ91 Alloy Fabricated by Rapidly Solidified Flaky Powder Metallurgy and Hot Extrusion. Metals and Materials International, 2019, 25, 372-380. Enhancing yield strength by suppressing detwinning in a rolled Mg–3Al–1Zn alloy with { <mml:math< td=""><td>1.8</td><td>22</td></mml:math<>	1.8	22
24	xmlns:mml="http://www.w3.org/1998/Math/MathML" altimg="si0002.gif" overflow="scroll"> <mml:mn>10</mml:mn> <mml:mover accent="true"&gt;<mml:mn>1</mml:mn><mml:mo>Â<sup>-</sup></mml:mo><mml:mn>2</mml:mn>twins. Materials Science &amp; amp; Engineering A: Structural Materials: Properties, Microstructure and</mml:mover 	2.6 \>}	20
25	Processing, 2014, 619, 328-333. Phosphorescence-Based Flexible and Transparent Optical Temperature-Sensing Skin Capable of Operating in Extreme Environments. ACS Applied Polymer Materials, 2021, 3, 2461-2469.	2.0	20
26	Effects of Laser Power on the Microstructure Evolution and Mechanical Properties of Ti–6Al–4V Alloy Manufactured by Direct Energy Deposition. Metals and Materials International, 2022, 28, 197-204.	1.8	20
27	Internal-variable analysis of high-temperature deformation behavior of Ti–6Al–4V: A comparative study of the strain-rate-jump and load-relaxation tests. Materials Science & Engineering A: Structural Materials: Properties, Microstructure and Processing, 2013, 562, 180-189.	2.6	19
28	Prediction of hole expansion ratio for various steel sheets based on uniaxial tensile properties. Metals and Materials International, 2018, 24, 187-194.	1.8	19
29	Plastic anisotropy of multi-pass caliber-rolled Mg alloy with split texture distribution. Materials Science & Engineering A: Structural Materials: Properties, Microstructure and Processing, 2020, 788, 139496.	2.6	19
30	Accelerating globularization in additively manufactured Ti-6Al-4V by exploiting martensitic laths. Journal of Materials Research and Technology, 2021, 12, 304-315.	2.6	16
31	Mechanisms of tensile improvement in caliber-rolled high-carbon steel. Metals and Materials International, 2012, 18, 391-396.	1.8	15
32	Phase transformation and its effect on mechanical characteristics in warm-deformed Ti-29Nb-13Ta-4.6Zr alloy. Metals and Materials International, 2015, 21, 202-207.	1.8	15
33	Role of deformation twins in static recrystallization kinetics of high-purity alpha titanium. Metals and Materials International, 2016, 22, 1041-1048.	1.8	15
34	Effects of carbon content on the tensile and fatigue properties in hydrogen-charged Fe-17Mn-xC steels: The opposing trends. Materials Science & Engineering A: Structural Materials: Properties, Microstructure and Processing, 2018, 724, 469-476.	2.6	14
35	High strain-rate superplasticity of AZ91 alloy achieved by rapidly solidified flaky powder metallurgy. Materials Letters, 2019, 234, 245-248.	1.3	14
36	Orientation Dependence on Plastic Flow Behavior of Hydrogen-Precharged Micropillars of High-Mn Steel. Metals and Materials International, 2020, 26, 1741-1748.	1.8	13

TAEKYUNG LEE

#	Article	IF	CITATIONS
37	Microstructural evolution and mechanical properties of nanocrystalline Fe–Mn–Al–C steel processed by high-pressure torsion. Materials Science & Engineering A: Structural Materials: Properties, Microstructure and Processing, 2021, 827, 142073.	2.6	13
38	Accelerated recrystallization behavior of commercially pure titanium subjected to an alternating-current electropulse. Journal of Materials Research and Technology, 2021, 15, 5706-5711.	2.6	13
39	Effects of Tungsten Addition on the Microstructure and Mechanical Properties of Microalloyed Forging Steels. Metallurgical and Materials Transactions A: Physical Metallurgy and Materials Science, 2013, 44, 3511-3523.	1.1	12
40	Brazing method to join a novel Cu <sub>54</sub> Ni <sub>6</sub> Zr <sub>22</sub> Ti <sub>18</sub> bulk metallic glass to carbon steel. Science and Technology of Welding and Joining, 2017, 22, 714-718.	1.5	12
41	Effect of type-C liquid metal embrittlement on mechanical properties of spot-welded TRIP steel. Journal of Materials Research and Technology, 2021, 13, 2482-2490.	2.6	11
42	Tempcore Process Simulator to Analyze Microstructural Evolution of Quenched and Tempered Rebar. Applied Sciences (Switzerland), 2019, 9, 2938.	1.3	10
43	Prediction of Electropulse-Induced Nonlinear Temperature Variation of Mg Alloy Based on Machine Learning. Journal of Korean Institute of Metals and Materials, 2020, 58, 413-422.	0.4	10
44	Origin of superior low-cycle fatigue resistance of an interstitial metastable high-entropy alloy. Journal of Materials Science and Technology, 2022, 115, 115-128.	5.6	10
45	Tuning the texture characteristics and superelastic behaviors of Ti–Zr–Nb–Sn shape memory alloys by varying Nb content. Materials Science & Engineering A: Structural Materials: Properties, Microstructure and Processing, 2022, 845, 143243.	2.6	10
46	Effect on Zn on Microstructures and Mechanical Properties of Mg–Gd–Y–Zn LPSO Alloys. Metals and Materials International, 2022, 28, 2613-2620.	1.8	9
47	Microstructural Influence on Stretch Flangeability of Ferrite–Martensite Dual-Phase Steels. Crystals, 2020, 10, 1022.	1.0	8
48	Effect of undissolved Nb carbides on mechanical properties of hydrogen-precharged tempered martensitic steel. Scientific Reports, 2020, 10, 11704.	1.6	8
49	Variation in Mechanical Properties of Ti-13Nb-13Zr Depending on Annealing Temperature. Applied Sciences (Switzerland), 2020, 10, 7896.	1.3	8
50	Enhancing Superplasticity of Ultrafineâ€Grained Ti–6Al–4V without Imposing Severe Plastic Deformation. Advanced Engineering Materials, 2019, 21, 1800115.	1.6	7
51	Improved cold-rollability of duplex lightweight steels utilizing deformation-induced ferritic transformation. Materials Science & Engineering A: Structural Materials: Properties, Microstructure and Processing, 2019, 742, 835-841.	2.6	7
52	Kinetics of Capability Aging in Ti-13Nb-13Zr Alloy. Crystals, 2020, 10, 693.	1.0	7
53	Integrated constitutive model for flow behavior of pure Titanium considering interstitial solute concentration. Metals and Materials International, 2014, 20, 1017-1025.	1.8	6
54	Tribological and corrosion behaviors of warm- and hot-rolled Ti-13Nb-13Zr alloys in simulated body fluid conditions. International Journal of Nanomedicine, 2015, 10 Suppl 1, 207.	3.3	6

TAEKYUNG LEE

#	Article	IF	CITATIONS
55	Deep-learning approach to predict a severe plastic anisotropy of caliber-rolled Mg alloy. Materials Letters, 2020, 269, 127652.	1.3	6
56	Prediction of Tempcore Rebar Strength Using a Thermomechanical Simulator with a Designed Hollow Specimen. Steel Research International, 2020, 91, 1900520.	1.0	5
57	Ambivalent Role of Annealing in Tensile Properties of Step-Rolled Ti-6Al-4V with Ultrafine-Grained Structure. Metals, 2020, 10, 684.	1.0	4
58	Interface Characterization of Al–Cu Microlaminates Fabricated By Electrically Assisted Roll Bonding. Journal of Micro and Nano-Manufacturing, 2017, 5, .	0.8	3
59	Sinter-joining of Cu54Zr22Ti18Ni6 BMG powder to Cu powder by spark plasma sintering. Materials Letters, 2019, 242, 55-57.	1.3	3
60	Microstructural Evolution of Multi-Pass Caliber-Rolled Mg–Sn and Mg–Sn–Mn Alloys. Metals, 2020, 10, 1203.	1.0	3
61	Manufacturing of a corrugated double-layered tube for the high-performance compact heat exchanger. International Journal of Advanced Manufacturing Technology, 2021, 112, 2065-2080.	1.5	3
62	Polyvinyl pyrrolidone ( <scp>PVP</scp> ) as an efficient and biocompatible binder for metal alloy processing: A case study with <scp>Tiâ€20Zrâ€11Nbâ€3Sn</scp> . Journal of Applied Polymer Science, 2022, 139,	, 1.3	3
63	Superior bonding properties of dissimilar steel joint produced by electroslag remelting. Metals and Materials International, 2015, 21, 1054-1060.	1.8	2
64	Effects of drawing strain and post-annealing conditions on microstructural evolution and tensile properties of medium- and high-carbon steels. Metals and Materials International, 2017, 23, 1176-1187.	1.8	2
65	Microforming of fine metallic rods by the selective laser melting of powder. Additive Manufacturing, 2020, 36, 101612.	1.7	2
66	Graded Grain Structure to Improve Hydrogen-Embrittlement Resistance of TWIP Steel. Crystals, 2020, 10, 1045.	1.0	2
67	Effect of Type-B liquid metal embrittlement cracks on high-cycle fatigue properties of spot-welded 1180 TRIP steel. Science and Technology of Welding and Joining, 2021, 26, 173-179.	1.5	2
68	Phosphorescence-based temperature and tactile multi-functional flexible sensing skin. Sensors and Actuators A: Physical, 2021, 332, 113205.	2.0	2
69	Constitutive Analysis of the Anisotropic Flow Behavior of Commercially Pure Titanium. Applied Sciences (Switzerland), 2020, 10, 7962.	1.3	1
70	Effects of Substitution of Y with Yb and Ce on the Microstructures and Mechanical Properties of Mg88.5Zn5Y6.5. Metals, 2021, 11, 31.	1.0	0